Title: Coloring Single Nanoparticle Trajectory on Live Cell Membrane with its Own History: a Presuppositionless Approach

Hansen Zhao[1], Zhenrong Huang[1,2], Feng Ge[1,3], Xiangjun Shi[4], Bin Xiong[2*], Xuebin Liao[4], Zonghua Wang[3], Sichun Zhang[1], Xinrong Zhang[1*], Yan He[1*]

[1]Department of Chemistry, Tsinghua University, Beijing, 100084, P. R. China.

[2]State Key Laboratory of Chemo/Biosensing and Chemometrics, College of Chemistry and Chemical Engineering, Hunan University, Changsha, 410082, P. R. China.

[3]Shandong Sino-Japanese Center for Collaborative Research of Carbon Nanomaterials, College of Chemistry and Chemical Engineering, Qingdao University, Qingdao, Shandong, 266071, P. R. China.

[4]School of Pharmaceutical Sciences, Collaborative Innovation Center for Diagnosis and Treatment of Infectious Diseases, Key Laboratory of Bioorganic Phosphorus Chemistry & Chemical Biology (Ministry of Education), Tsinghua University, Beijing 100084, P. R. China.

*Correspondence to: yanhe2021@mail.tsinghua.edu.cn; xbcs1985@hnu.edu.cn; xrzhang@mail.tsinghua.edu.cn

Abstract: Single particle tracking has long been utilized for investigation of complex system dynamics such as nanoparticle-cell interaction, and the analysis of complicated behaviors of individual particles is always an outstanding issue. Existing methods treat each data point or short fragment on the recorded trajectory as an isolated "atom" and determine their relationship by using externally predefined mechanical models or physical states, which inevitably lead to oversimplification of spatiotemporal complexity. Herein, inspired by the phenomenology study in philosophy, we propose a machine-learning-based modeless framework to analyze single particle trajectories. This new strategy consists of 3 steps: 1) make the atomic data-points on the entire trajectory all connected by constructing successive overlapped historical vectors; 2) perform unsupervised clustering in the huge vector space to find their relative differences; 3) project the differences back to the trajectory for data visualization. Consequently, the inner heterogeneity of the spatiotemporal data object emerges on its own as a colored trajectory, exhibiting both a global picture and the details on local transitions of the particle movement, without the need to predefine any models, parameters or training sets. We demonstrated with simulated data that the underlying mechanism of various time-series of single particle motion could be well resolved in a consistent manner. Experimentally, we collected time-series data of lateral positions and orientations of single gold nanorods, and demonstrated that our analysis method could reveal the motion states and detailed dynamics of the nanoparticles during their entire transmembrane process. Since it is becoming increasingly difficult to find mechanical-model-based solutions for complexity studies at various scales, and the dynamic behaviors of individual molecules, particles, biological cells, cars and even stars could all be reduced to spatiotemporal trajectories of "single particles", this presuppositionless approach could help the fundamental researches on many important systems.

1. Introduction

Investigation of the interactions between nanoparticles (NPs) and the live cell membrane are crucial in the understanding of critical biological processes such as nanoparticle cytotoxicity (1), drug delivery (2, 3), gene therapy (4, 5) and cellular endocytosis (6). Toward this end, tracking and analyzing the motions of individual nanoparticles in situ in real time, which could provide the spatial and temporal distribution of heterogeneity associated with the complex environments on cell surface, has attracted continuous interest (7-9). Taking advantages of rapid developments of optical imaging methods, researchers have been able to obtain the spatiotemporal series of multiple feature parameters such as the fluorescence and scattering intensities, the spectra and colors (10), and the rotation and orientation angles of individual NPs (9, 11, 12). However, the efforts to extract meaningful information and uncover the complex physical and biological mechanisms are always entangled with the stochastic natures of the NP motion, transient NP interaction with cell surface (13, 14), and varying distribution of surface micro-domains as well as the detection error. It is therefore a fundamental problem to analyze and extract physical and biological meaningful information from the single NP trajectories.

Given the high spatiotemporal complexity of NP-cell interactions, the primary issue is to find an appropriate approach to differentiate and describe the particle movement. To begin with, conventional methods usually need to predefine the local environments and external forces that surround and restrict the single NPs, i.e. the motion-states the NPs could exhibit, and stipulate a framework based on a priori physical models. The data for analysis are generated from the particle trajectory using subsequence or moving window operation. The general assumption is that during the NP-cell interaction process, the NP motion states within a short time window is either stable or statistically predictable, and different NP states are independent and limited in number (15). These underlying states could be recovered by either numerical fitting or by machine learning based model assignment, where the temporal sub-trajectories are treated as atomistic fragment or event and are generally thought isolated from the previous and later ones. For example, by assuming that mean-square-displacements in the subsequence could be described by the general equation for anomalous diffusion, different particle states could be separated based on empirically determined thresholds of the diffusion coefficients and asymmetry factors (16). Alternatively, by assuming the whole trajectory being a Markov process containing multiple states, and pre-estimating the initial state probability, emission probability and state transition probability, the hidden Markov model (HMM) method could be used to evaluate the sequence of the hidden states step-by-step and infer the underlying mechanism of the particle motion (17, 18). To relax the prerequisite on either numerical or statistical description of the transient dynamics, some people resort to supervised clustering. Using empirically selected or simulated sub-trajectories to feed the classifier in advance, support vector machine (19), random forest (20) and Bayesian inference (21) have been proved to be reliable for dynamic state sequence differentiation. All these reductive strategies are largely applicable to reveal the general characteristics of the system embedded in the NP trajectories, but the pre-assumptions on a priori states or models often suffer from oversimplification or loss of individuality of the NP-cell interactions that are intrinsically heterogeneous and dynamic in time and space.

To analyze a complicated dynamic process over time without predefined models or external criteria, we have to establish a presuppositionless strategy that have the internal states or inner differences emerge on their own. While this possibility has not been considered seriously in physical-model based fundamental research until very recently, the corresponding issue in

philosophy, namely how to “return to things themselves”, has been examined in-depth for centuries by European philosophers. One of the central issues is the phenomenology of time-consciousness, i.e. how a chronological object occurs across successive moments appears to people as the temporal unity of multiple consecutive temporal states (22). For example, a person is enjoying a beautiful melody never heard before. How can he perceive detailed changes of the music while enjoying the overall beauty of the melody? Obviously, these perceived details in sound are arranged sequentially over time, but neither are monotonous notes nor mechanical combinations of notes, and cannot be pre-communicated with “musical models”. According to the phenomenology studies, at each time point, the basic unit of perception is not an atomistic moment irrelevant to others, but a conscious experience-fragment with some temporal depth anchored by the current point. Each experience fragment is composed of a certain number of consecutive moments before that point, so the successive experiences are different, but are interrelated due to their overlap in time. Such “succession of experiences” is the foundation by which the physical time and temporal change can be perceived. However, without a predefined a priori criterion, just a sequence of experiences of isolated short musical fragments are not sufficient to produce the perceived musical unity as well as the detailed states on the melody. Hence, a special operation at a higher conscious level is necessary to differentiate the short experience-fragments from each other, and simultaneously coalesce them in the temporal order, so that the person can actually “experience the succession” or perceive the temporality of the melody. Such an operation, capable of revealing the past, present and future phases of a temporal object while itself surpassing the chronological order, is postulated as an inner logical structure of consciousness (e.g. the tripartite form of retention-primal impression-protention proposed by Husserl). Probably due to the difficulty in making objective empirical verifications, however, the philosophers can hardly give a very clear and satisfactory account on this issue.

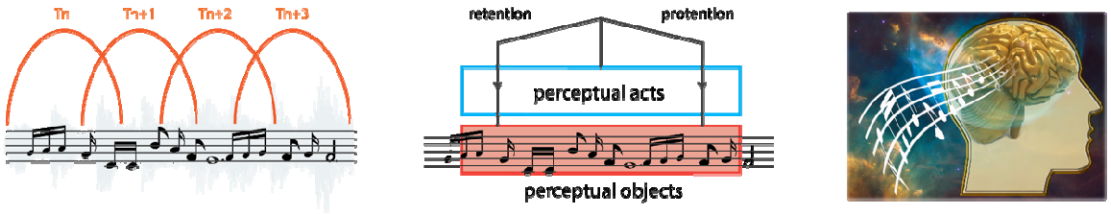

Fig1. The phenomenology of time-consciousness, using enjoying music as an example. (left) A melody can be represented as a collection of isolated notes, but the basic unit of perception is overlapped experience-fragments; (middle) a higher-level conscious structure is needed to (right) enjoy both the detailed rhythm and overall beauty of the melody.

The coming of Data Era makes it possible to combine data science and fundamental research on complex dynamic systems at the modeless phenomenology level (23-25). Data are acquired objectively, but are little meaningful without being interpreted or visualized appropriately. Unlike ordinary things that are intuitively perceivable, data processing usually needs explicit subjective-objective unification. If the data is highly fragmented or the amount of data is very limited, people would have to resort to some predefined prototypes to rationalize the otherwise seemingly clueless data points or fragments. With the size of available data growing fast exponentially, people have already been using data-driven approaches and “having the data speak for themselves” via all kinds of data-science and data-visualization tools (26, 27). However, the current data-driven

techniques are developed mainly at the application level and there is so far little consensus on the methodological foundation of the Data-Science. Inspired by the phenomenology on time-consciousness studies, in this work we propose a new strategy to uncover the spatiotemporal structures of single particle trajectory data. We treat a trajectory as if it were a nanoscale melody having been experienced by the particle. To reveal the detailed states of the particle motion as well as their change over time as a unity, we conceptualize a special data processing operator composed of 3 steps. 1) Construct a succession of overlapping experience-fragments of the particle with a specific predisposition. 2) Perform internal comparison or unsupervised clustering of all the experience-fragments to obtain the relative differences among themselves. 3) Color the trajectory accordingly to generate the perceivable experience of succession through segmentation of the particle motion. Compared with phenomenological description at the subjective conscious level, the key aspect of the 3-step operator is still the transformation from the "succession of experience" to the "experience of succession" (SEES), but is performed at the objective data level and is empirically reproducible. Additionally, just like musical analysis, the resulting trajectory with multiple color segments can be further analyzed to extract more specific information with supplemental knowledge on the time series data. We demonstrate with both simulated and experimentally obtained NP trajectories that, after applying the pressuppositionless SEES operator, the dynamic spatiotemporal states of NP-cell interactions could be successfully unveiled. This generalized modeless data-phenomenology framework could promote the application of data-driven techniques in complexity studies.

2. Description of the SEES Method

The first step of the SEES operator is to construct a succession of short experiences out of the single particle trajectory. The key here is not to view a trajectory obtained from a complex system as a simple assembly of separated atomistic events bound by fixed external laws or mechanical states, but as a consecutive sequence of cross-related historical experiences anchored by their current points. Each current-point carries an experience-fragment composed of its past points, and itself is also the immediate past point in the experience-fragment of the following point, and so on. This step is technically similar to the sliding window operation but is conceptually different. The later usually only intends to reduce noise from the data, and still treats each window as an isolated atomic fragment that can be collapsed into either a fixed value by averaging or a predefined kinetic phase by fitting, which inevitably suffers from information loss. The former treats each fragment as a temporal vector that keeps the chronological order of the data points, in which all the dynamic information is preserved. We note that while building the sequence of experience-vectors does not need predefined a priori models, it cannot be done without certain "intention" that is based on the prior knowledge of the system. Just as there are many perspectives to looking into the history of an individual, in what aspect the researcher intends to investigate determines how to generate the experience-vectors. For a single NP trajectory, we can focus on different features of the particle such as its velocity or orientation angle values, its rotational diffusion rate, and its spatial confinement, etc., and construct the experience-vector sequence accordingly. Since the purpose is to differ them internally, the historical length of the vectors is not crucial as long as it reaches a minimum. To select the appropriate value, well-developed non-linear time series analysis methods such as the Cao method (28) and the mutual information method (29) can be applied to provide a meaningful initial estimation, though the NP-cell interactions may not be chaotic.

The second step of the operator is to find the inner difference within the sequence of the NP experience-vectors. The corresponding stage in the phenomenology of time-consciousness is highly intriguing, as it is difficult to imagine or justify the existence of a special higher-level conscious operation that has the ability to differentiate various temporal phases from the succession of conscious experiences. However, this is not a problem at the data level since it is not necessary to stick to the temporal order of the NP experience-vectors during data processing, and each vector can be compared with all the others simultaneously via a number of machine-learning based techniques. Here, we chose the basic unsupervised k-means clustering method just to prove the concept. With the whole set of historical experience-vectors as the input, the output is the high-dimensional vector space being partitioned into a few categories with their cluster center. The criteria or metrics for the partitioning can be set based on the construction of the historical experience-vectors and the feature to be probed. The appropriate number of categories can be estimated according to the literature (30). We note that such action is similar in certain extent to the subsequence time series clustering, which has been reported to be inefficient in revealing the true physical structure of some types of time series (31). However, instead of focusing on the physical importance of the cluster centers, what the SEES operator does at this step is just to have their differences emerge but not necessarily to justify their physical nature. It is because that as internal comparison without a priori criteria, the differences between cluster centers are only relative and the classification of each experience-vector is probabilistic. To make the clustering results physically meaningful, their difference must be mapped back to the original spatiotemporal trajectory of the particle, and that leads to the next step of the operator.

The third step is to color the single NP trajectory according to the clustering difference. By assigning each cluster of experience-vectors a color and labeling every point on the trajectory using the color of the vector it carries, we obtain a trajectory labelled with multiple colors. Because of the existence of both local consistency and global difference, the same color points on the trajectory are usually not randomly distributed; they tend to assemble locally into multiple color segments, resulting in the emergence of a collective pattern of color continuities. The visually perceivable "experience of the succession" within each color segment could be attributed to the single NP continuously experiences similar motion patterns or surrounding environments in time and space, and can be specified as a local state with a non-zero temporal depth. Hence the sequence of color change exhibits the variations and dynamic transitions of the local states. We note that although the algorithm ensures it reproducible, the classification of an experience-vector is not deterministic but probabilistic, thus the temporal length and the boundaries of a color segment or the appearance of a local state are also probabilistic. However, such uncertainties are not stochastic and are linked globally by the wholeness of the trajectory, and the nondeterministic picture is consistent with the complex nature of NP-cell interactions. After all, for a complicated dynamic process, the primal issue is to obtain the spatiotemporal transitions and the general distributions of different local states. The physical characteristics of each state could be further analyzed based on previous knowledge on the process.

Taken together, from the "succession of experiences" to the "experience of succession", the whole procedure performed by the 3-step SEES operator on the single particle trajectory is essentially the "negation of the negation" of the momentary movements of the particle. Unable to rely on a priori models but still taking the entire trajectory as a unity, an individual moment can only find its relative "truth" via making active connections to all others. Making an argument similar to the dialectic in Hegel's *Phenomenology of Spirit*, firstly, to construct the historical experience-vector

is the “negation” of atomicity of the individual “now” moment, and disburses its zero dimensional information into a high dimensional space. The appearance of every moment in continuous tens of vectors and the heavy overlap between adjacent vectors ensure the plurality of the “negation” action and make them all connected. Secondly, the unsupervised clustering, carrying a particular predisposition from the observer, drives each individual vector to compare with all others universally and find out their relative position by using other vectors as “mirrors”. Finally, by coloring every momentary point on the NP trajectory according to the category of its leading vector, the first “negation” is “negated” again, and the added information from vectorization and universal comparison is “reflected” back into the original individual moment itself. The high dimensional space is reduced back to the low dimensional space, and the global clustering difference is projected onto the localized spatiotemporal difference. Such a dialectic circle, from the momentary individuality to the universality of the whole trajectory and then back to the individuality, is achieved through the particularity of all the individuals’ own history rather than through externally defined mechanical models. Consequently, a continuous “change of change” of the single particle movement both globally and locally is exhibited in the form of a colored trajectory, which is just like the details as well as the unity presented aurally by a music. To our knowledge, it is the first time that the famous “negation of the negation” dialectic principle, supported by the machine learning technique, finds a practical implementation in fundamental scientific research. Alternatively, since extensive vectorization, universal comparison, and certain reflection are the common aspects of almost all machine learning techniques, the “negation of the negation” dialectics probably underlies the effectiveness of the methodological foundation of the Data-Science.

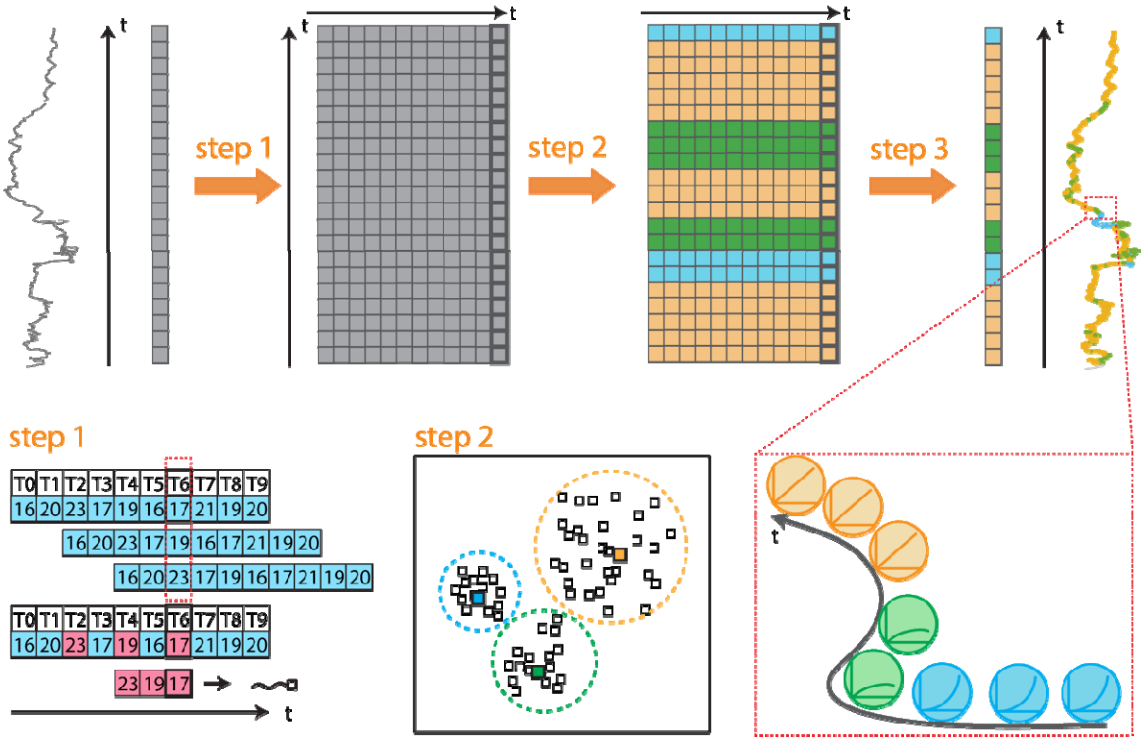

Fig2. The 3-step SEES operator: step 1, construct the sequence of historical experience-fragments by the time-lag operation; step 2, apply k-means unsupervised clustering to differentiate the experience-vectors in high dimensional space; step 3, map the color tags of the clustering results back to the trajectory. The

color fragments formed can then be analyzed by using existing physical models.

3. Method Evaluation

The implementations of the SEES operator, including constructions of the experience-vectors from a NP trajectory and the partition metrics in the k-means clustering algorithm, are provided in the Note S1. Briefly, to process the time series of both the lateral position and orientation angle of a nanoparticle, we provided 3 options of vector construction. The univariate (U) extracts directly the sub-trajectories from the time series. The mean-square-displacement (MSD) and the autocorrelation (AC) focuses on the local spatial confinement and the fluctuation frequency of the sub-trajectories, respectively. As metrics for comparison of vector similarity, we used either Euclidean distance (ED) or cross-correlation (CC), which are sensitive to their numerical closeness and the variation trend, respectively.

In order to validate the method before using it to process the experimental data, we applied the SEES operator to simulate spatiotemporal series data with known ground truths (Note S2). To examine the robustness and universal applicability of the operator, we generated 3 cases with totally different underlying physical mechanisms. The first example is a nanorod both rotating and revolving around an external axis simultaneously. The time-series obtained is the projection of its trajectory on one dimension, exhibiting both a local and a global periodic sinusoidal pattern. Targeting the tendency of data variation, we performed the SEES/U-CC operation. The resulting cluster centers indicate that the experience-vectors of the nanorod are correctly partitioned into two groups of ascending and descending tendency without physical or statistical presumption, and the periodical variation of the trends are rightly captured by the spontaneous accretion of the same color points on the colored trajectory.

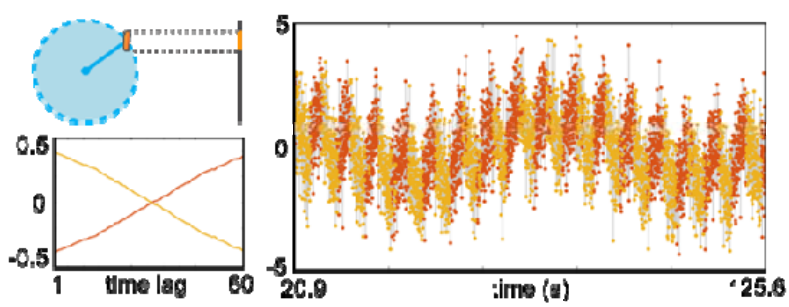

Fig3. Nanorod rotation/revolution provides sinusoidal observations. The SEES/U-CC operation successfully revealed the periodic pattern and differentiated the ascending and descending tendency.

In the second case, we simulated a trajectory of a NP diffusing on a 1D membrane, whose moving rate varies at different regions due to the heterogeneity of the local environment. We applied the SEES/U-ED operator to the time series of NP velocity. With the historical experience-vector

length increasing from d=1 to 30, we can see how the underlying temporality of the NP motion emerges from the time-series gradually. When d is small, no clear pattern appears due to the stochastic nature of the transient NP rates. Increasing the vector length to 10 leads to a much better estimation of the transition of the diffusion states but still contained confusions. As d=30, the mean values of the cluster centers accurately match the ground truth. The resulting colored trajectory and spatiotemporal distribution of the color fragments are consistent with the original simulated one. The vector of the cluster center in each category shows approximately a flat curve whose mean value is comparable to the theoretical calculation according to the simulation. Surprisingly, not only the long regions but also the short regions of NP velocity variation are successfully recovered, though the boundaries and a few details are not precise. Close examination of the simulations with various NP diffusion coefficients and region sizes as input (Fig. S1) indicate that such good match could be attributed to the advantages of the large data set and the huge number of vector comparisons performed in the high dimensional space according to the Law of Large Number. Most of the physical models on single particle movements used nowadays were developed at times when the data acquisition and processing techniques were limited. Therefore, it is the data size that makes the presuppositionless SEES operator applicable.

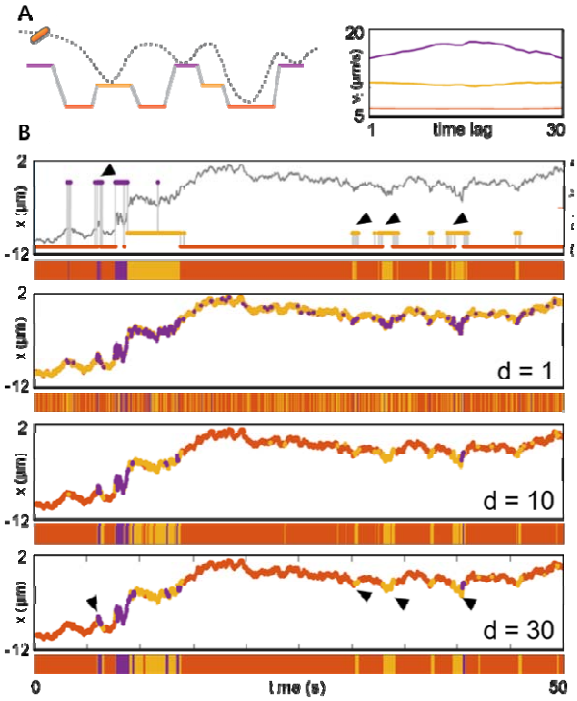

Fig4. (A) Nanoparticle diffusion on a spatial heterogeneous 1D membrane. The schematic diagram of the model (left panel) and the cluster centers of the SEES/U-ED operation with vector length of 30. (B) The ground truth of the time series of NP velocity (row 1) and the results processed using the SEES/U-ED operator with the length of experience-vector, d, being set at d=1 (row 2), d=10 (row 3) and d=30 (row 4). When d=30, the clustering centers show high consistency to the expected mean velocities.

In the third example, we simulated a NP diffusing on a 2D cell membrane where a number of binding regions with different affinities distributed randomly. The NP jumps into or out of the

confined regions randomly and undergoes confined or directed motions, respectively, producing a continuous trajectory. The possibility of state switching is not static throughout the process and does not depend on the immediately preceding state, but rather on the spatial location of the NP, and more specifically, the binding affinity of a particular region (Note S2). Hence the state transition probability deviates from the basic assumption of HMM, but it has a clear biological significance: NPs coated with specific antibodies are more likely to bind to their corresponding antigens than other membrane proteins, and it is more difficult to escape from immune binding.

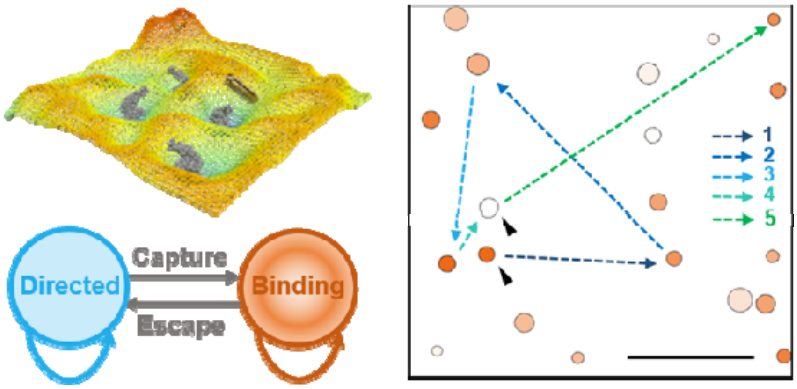

Fig5. Binding/dissociation model simulates a nanoparticle interacting with a 2D cell membrane. Nanoparticles can switch between binding state and directed motion (dissociated) state depending on the spatial position. Binding sites with different local properties spread randomly on the surface marked by green color. The dash line arrows show the jumping trace of the nanoparticle from 10 s to 60 s of the simulation.

However, we could handle this situation by using two modeless SEES operators simultaneously. The SEES/MSD-ED operation on the NP position is sensitive to the historical confinement of the particle and indeed reveals the binding regions where the NP exploited. Meanwhile, the SEES/U-ED operation on the NP velocity series is more sensitive to the local diffusion coefficient inside the binding region (Fig6.A, S2). Although the local diffusion coefficients are simulated to vary continuously within a certain range (Note S2), just categorize the historical vectors of NP velocity into 3 clusters is enough to largely separate the regions of different binding affinity. As shown in Fig6.B, the 3 colors of purple, yellow and orange represent the NP velocity is high, medium and low, respectively. The segments where the NP undergoes directed motion is colored mainly purple. The regions where the NP binding occurs are colored mostly orange and yellow but of different portions, revealing their different binding affinity. Therefore, the combined SEES/MSD-ED and SEES/U-ED operations on the two observed variables (NP position and NP velocity) reveal both the locations and the affinity variations of the binding regions, providing a comprehensive description of the NP motion.

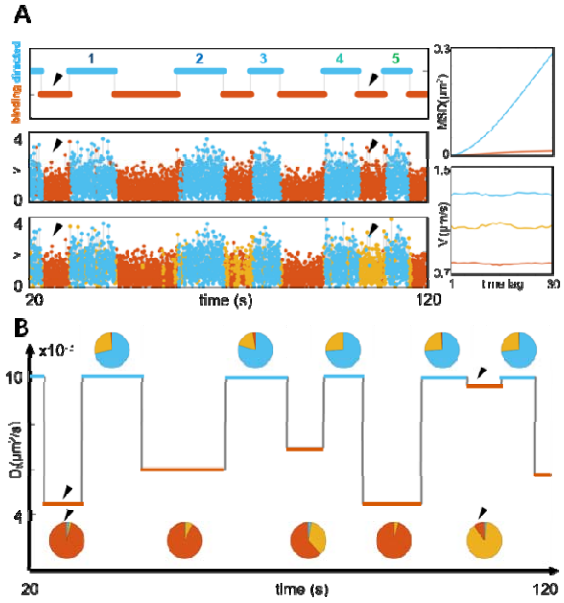

Fig6. (A) Given the ground truth (row 1), the SEES/MSD-ED operator using 2 clusters differentiated the binding state and the directed motion state of the NP dynamics (row 2). The SEES/U-ED operator using 3 clusters further revealed the heterogeneity of the binding sites (row 3). The cluster centers of these two operations were displayed in the right panel. More details on the simulations are provided in Supplementary Note S2. (B) The calculated local diffusion coefficients and the percentage distribution of the vector colors in each segments obtained from the SEES/MSD-ED operation. Black arrow indicates two binding sites with different local diffusion coefficient.

Altogether, though the physical pictures of the above 3 simulations differ considerably, the underlying NP dynamic states and state transitions were all successfully recovered by using the modeless SEES operator. For comparison, when applying the SEES operator to the simulated trajectory of a purely random walker with no motion state variation, no self-aggregated color segments is observed and different points on the trajectory are colored randomly regardless the length of historical experience vectors (Fig. S3). Thus, the coloring profiles resulting from the SEES operator can only came from the real differences in the particle dynamics embedded in the particle trajectories. Since the SEES operation is capable of handling not only classical heterogeneous processes with just one temporal variable, but also more complicated processes with multiple time-dependent parameters, this strategy may provide a new option for dealing with the multivariate big data.

4. Experiment: Single Nanoparticle Dynamics on Live Cell Membrane

To investigate the dynamic interactions between nanoparticles and cells, we monitored the entire transmembrane process of single gold nanorods (AuNRs) and resolved the corresponding diffusion dynamics with this modeless strategy. The SPT experiment was performed under a darkfield microscope equipped with a color CMOS camera. Because the diffusive and rotational behaviors are key parameters that can affect the nanoparticle fate in cell membrane (11, 32), we have developed a simple and effective method to simultaneously track translational and rotational motion of single AuNRs at the live cell surface based on the analysis of particle localization and out-of-plane

angle-dependent scattering color

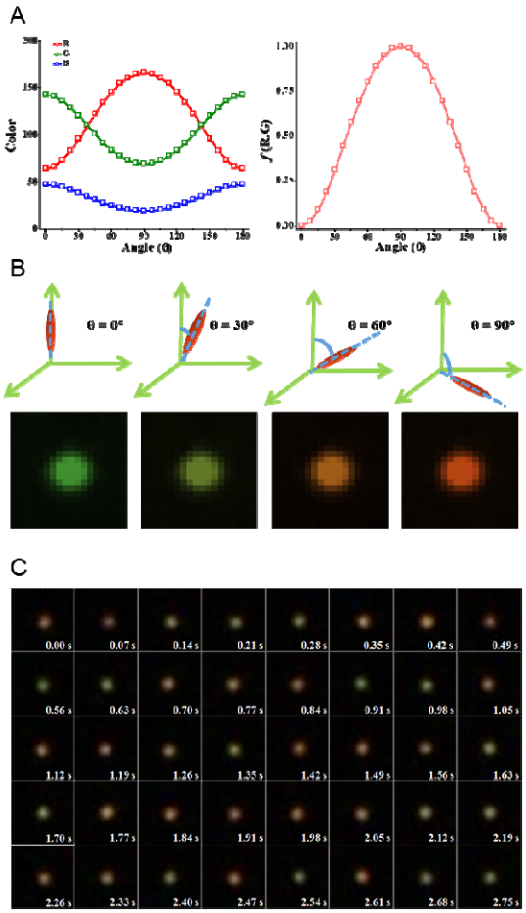

Fig7. Out-of-plane angle of AuNR determination by color change. (A) Simulated darkfield image intensities of single AuNR obtained from the R, G and B channels of the color CMOS camera as a function of the out-of-plane polar angle θ and the polar angle dependence =sin2θ. (B) Typical AuNR polar angle orientations and the corresponding simulated color images. (C) Typical image sequence of a single AuNR rotated in 99.5% glycerol-water solution.

Fig8 displayed a complete trajectory of a RGD-modified AuNR entering the HeLa cell, which spanned nearly 9 minutes with over 8,000 data points. Intuitively, the spatiotemporal map could be divided into 5 local diffusional regions connected by 4 directional tracks (Fig8.A insert). To analyze the data, the conventional approach is to obtain the distributions of the AuNR angle, velocity and diffusion coefficient according to established physical models at the atomic-point or the sub-trajectory level with artificial segmentation or sliding window segmentation (Fig8). According to the multi-parameter information as well as the predefined criteria based on their variations, certain dynamic patterns, temporal segments or critical points of the particle motion can be identified and used to describe the behaviors of the transmembrane process (Table1). However, the raw AuNR trajectories recorded in the heterogeneous cellular environments are often highly complicated and are entangled with random noises, making it time-consuming to differentiate the dynamic states of the AuNR by studying the motion path of the particle visually even for trained technicians. As a result, personal experience based partition of the trajectory is often inefficient and irreproducible, and

inevitably leads to much subtle information unresolved or unobserved.

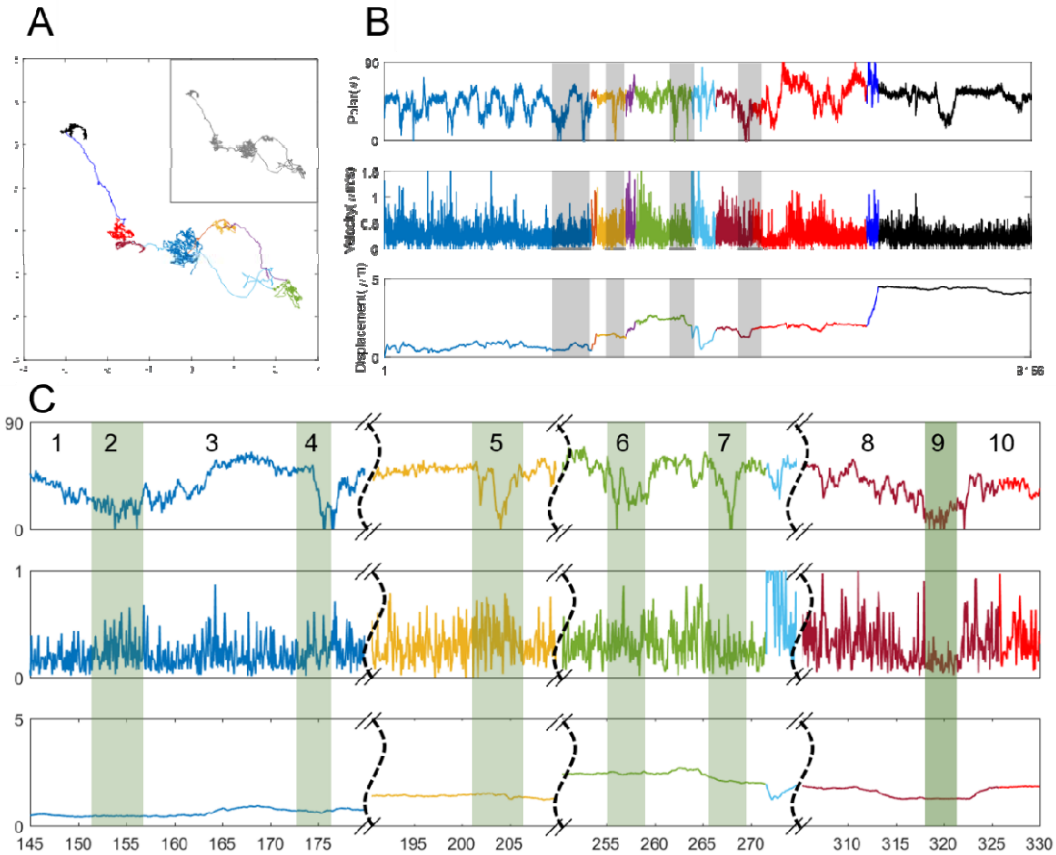

segment index	time from (s)	time to (s)	Velocity (μm/s)	polar angle	α	Dt ($\mu m^2/s$)	distance (μm)	displacement (μm)
1	140.00	152.60	0.20±0.14	37.83±9.94	1.05	0.0018	2.48	0.15
2	152.67	157.15	0.27±0.16	19.07±8.30	0.12	0.0002	1.24	0.04
3	157.22	170.03	0.21±0.14	43.50±14.49	1.47	0.0017	2.62	0.48
4	173.74	176.75	0.29±0.14	27.15±17.39	0.80	0.0012	0.87	0.07
5	201.32	205.94	0.39±0.20	34.94±14.36	1.51	0.0085	1.79	0.36
6	255.01	259.35	0.33±0.16	32.42±11.98	0.61	0.0016	1.45	0.03
7	266.00	269.50	0.24±0.13	37.20±14.89	1.10	0.0020	0.83	0.21
8	310.03	317.87	0.28±0.19	35.86±9.85	1.74	0.0035	2.21	0.48

segment index	time from (s)	time to (s)	Velocity (μm/s)	polar angle	α	Dt ($\mu m^2/s$)	distance (μm)	displacement (μm)
9	**317.94**	**322.00**	**0.16±0.13**	**13.06±6.74**	**0.18**	**0.0001**	**0.61**	**0.06**
10	**322.07**	**331.94**	**0.36±0.21**	**35.17±6.66**	**1.38**	**0.0036**	**3.59**	**0.62**

Fig8. Traditional manual trajectory segmentations and cell-entry point determination. (a) RGD-coated AuNR interacted with HeLa cell membrane shown in Fig3.C insert. Heterogeneous movement dynamics can be investigated by manual segmentation referring to the (b) polar angle, velocity and displacement time series profile. In this case, 6 diffusion states are linked by 4 directed states. (c) 10 regions were manually selected and their local physical properties were calculated as listed in table below. The cell entry site (region 9) was characterized with lowest mean velocity, lowest mean polar angle and confined movement.

Alternatively, the SEES method focuses on the variation trend associated with each spot rather than the atomic values, and are resistant to stochastic noises and local fluctuations. By processing the AuNR trajectory with the SEES operator, the segmentation of the NP trajectory and the classification of its motion states can be achieved directly through the resulting color-coded sequence, making it possible to analyze the diffusion statistics and reveal the transient heterogeneity of the NP-cell interaction dynamics. Fig9 show the colored out-of-plane angle and velocity time-series after the SEES/U-ED operations. The experience-vectors were both categorized into 5 groups based on their magnitude from small (orange) to large (blue), respectively, resulting in the spatiotemporal trajectory being partitioned into tens of segments whose time duration varies from 1.33 s to 42.63 s. Fig9.C shows the accordingly colored x-y trajectory. The emergence of the sequence of color segments of various lengths produced a perceivable vivid overall picture on the temporality of the AuNR motion, which is not available from the raw or intuitively divided trajectory. When varying the length of the experience-vector (Movie S3) or trimming from 2 ends of the time-series (Movie S4), the overall coloring scheme from the SEES operation remains largely unchanged, as long as the vector length and the data size exceed some threshold. Therefore, the robustness and the reproducibility of the segmentation are guaranteed, and the SEES operation reveals true motion states of NP-cell interaction. For each segment, we can further calculate the feature parameters such as the average velocity, mean orientation angle, lateral and rotational diffusion coefficient, and anomalous factor of the particle during that period, respectively, according to established physical models. They provide transient NP dynamics and could serve as quantitative measures and statistical evaluation of the segments in the feature space. Such highly divided and uneven segmentation revealed the inner difference of the entire spatiotemporal process, which would not be achieved with artificial or sliding window subdivision.

The SEES operation makes it easy to identify the spatiotemporal position of the transmembrane event. From the segmented out-of-plane angle and velocity time-series in Fig9, it is clear that the translational and rotational motions of the AuNR near the cell surface are relatively independent in most situations. Nevertheless, the two types of motions became synchronous for a short duration at ~ frame 4,500, displaying a same orange color region simultaneously. At this unique region, the AuNR out-of-plane angle and velocity were both small, indicating the nanorod at its highest confinement and lowest speed and being vertically inserted into the plasma membrane, which matched well with

the reported situations of AuNR endocytosis (32). This cell-entry event was confirmed by the observation of directional transport of AuNRs after this region, which corresponds to molecular motor guided cargo transport after internalization by living cells. These findings suggested that the translational and rotational trajectory classifications under SEES operation make it easy for identification of the transmembrane sites of single AuNRs. By examining more single AuNR trajectories (Fig. S4 to S6), it turned out to be a correct measure in spotting the transmembrane sites and discriminate those particles that did not enter the cell, indicating the reliability of this data processing strategy. Furthermore, with the knowledge on the length of every tagged region, though only probabilistic, we could estimate the duration of single membrane-crossing events in an objective and reproducible manner. We determined the value to be ~6.9 s for RGD coated AuNRs and ~3.1 s cationic peptide coated AuNRs (Fig. S5 and Fig. S6). Therefore, the SEES segmentation provides a convenient method without modeling to determine the boundaries and transitions of single particle motion states in heterogeneous environments.

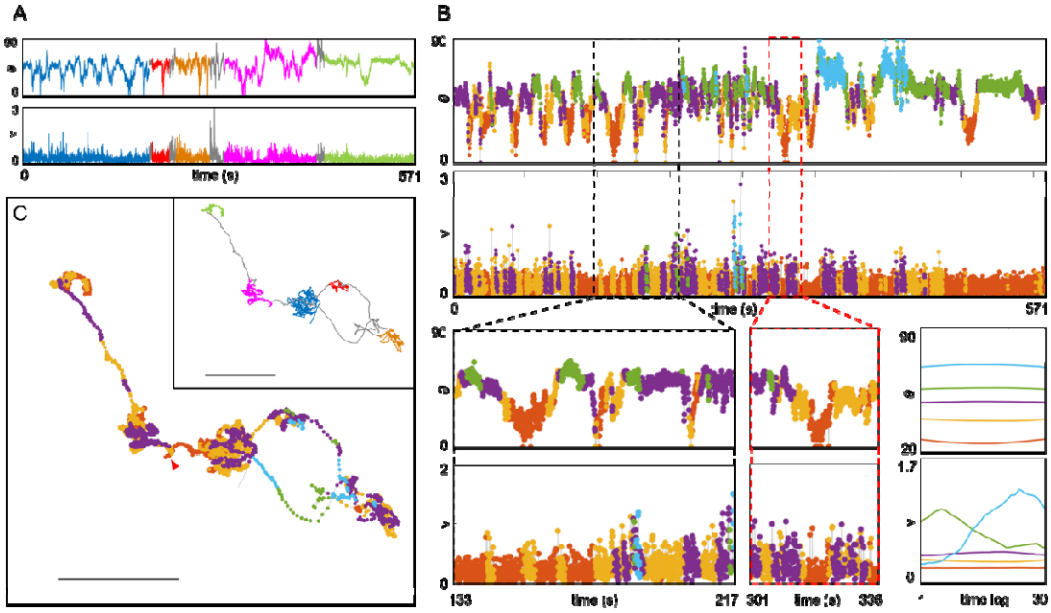

Fig9. Identification of the single AuNR transmembrane site. (A) Time series of the out-of-plane angle (upper) and velocity (lower) of the entire dynamic process of a RGD-modified AuNR interacting with and crossing the membrane of a HeLa cell. The color segmentations are consistent with the manual segmentation of the spatiotemporal trajectory in the C inert. (B) Color segmentations of the same time series of the out-of-plane angle and velocity of the AuNR after SEES/U-ED operation. The enlargement shows that the transmembrane site (red dash box) can be easily differentiated from other similar sites (black dash box) by the synchronic tagging of orange color in both series. Also shown to the right of the enlargement are the cluster centers of the SEES/U-ED operation on the polar angle series (upper) and velocity series (lower). (C) The corresponding colored spatiotemporal x-y trajectory of the AuNR after SEES/U-ED operation on its velocity time series. The insert is the manual segmentation. The scale bar is 2 μm.

The SEES operation also allows in-depth investigation of the AuNR diffusional states and their transitions during the entire NP transmembrane process, which reflects the heterogeneous NP binding to the highly compartmentalized but fluidic plasma membrane as well as the crowding of the intracellular environment. To study the lateral confinement of the AuNR, we applied the

SEES/MSD-ED operator to the AuNR x-y trajectory, where the sequences of experience-vectors were clustered into 5 groups according to the degree of local confinement (DLC) from high (orange) to low (blue) (Fig10). As shown in Fig10.B, before the transmembrane event, the orange regions with the highest lateral DLC were relatively dispersed and their length was relatively short. After that, the orange regions spanned longer time and were more aggregated, indicating the AuNR mostly stayed in a crowded intracellular environment. A close examination on the chronological evolution of the colored segments (Fig10.C and Movie S5) and the historical vectors (Fig10.D and Movie S6, S7) discloses a more vivid picture. It is apparent that the transient diffusive behaviors of the RGD coated AuNR on the compartmentalized cell membrane could be divided into two types of hopping and lingering before the cell-entry, though the duration and displacement of either mode fluctuates all the time. The lingering length is typically several μm, where the particle was probably trying to enter the cell. The jumping length ranges from a few to tens of μm, providing more opportunities for the ligands on the AuNR surface to bind with membrane receptors of other locations once the transient ligand-receptor engagement was not sufficient for receptor-mediated nanoparticle endocytosis. Through frequent and drastic diffusive state transition, the particle could search a large area within a short time and find its appropriate cell-entry point quickly. We confirmed this motion pattern by analyzing the diffusion of multiple AuNRs. Such a hop-and-linger mode is consistent with that the plasma membrane is using two mechanisms jointly to adjust its local composition for membrane compartmentalization: the formation of barriers that passively hinder free motion and the active delivery of components to specific locations (33). Since it can achieve reproducible identification of changes in the diffusive behavior and reliable recognition of clustering and transient confinement within single particle trajectories, the SEES operator could make it more convenient to study membrane trafficking.

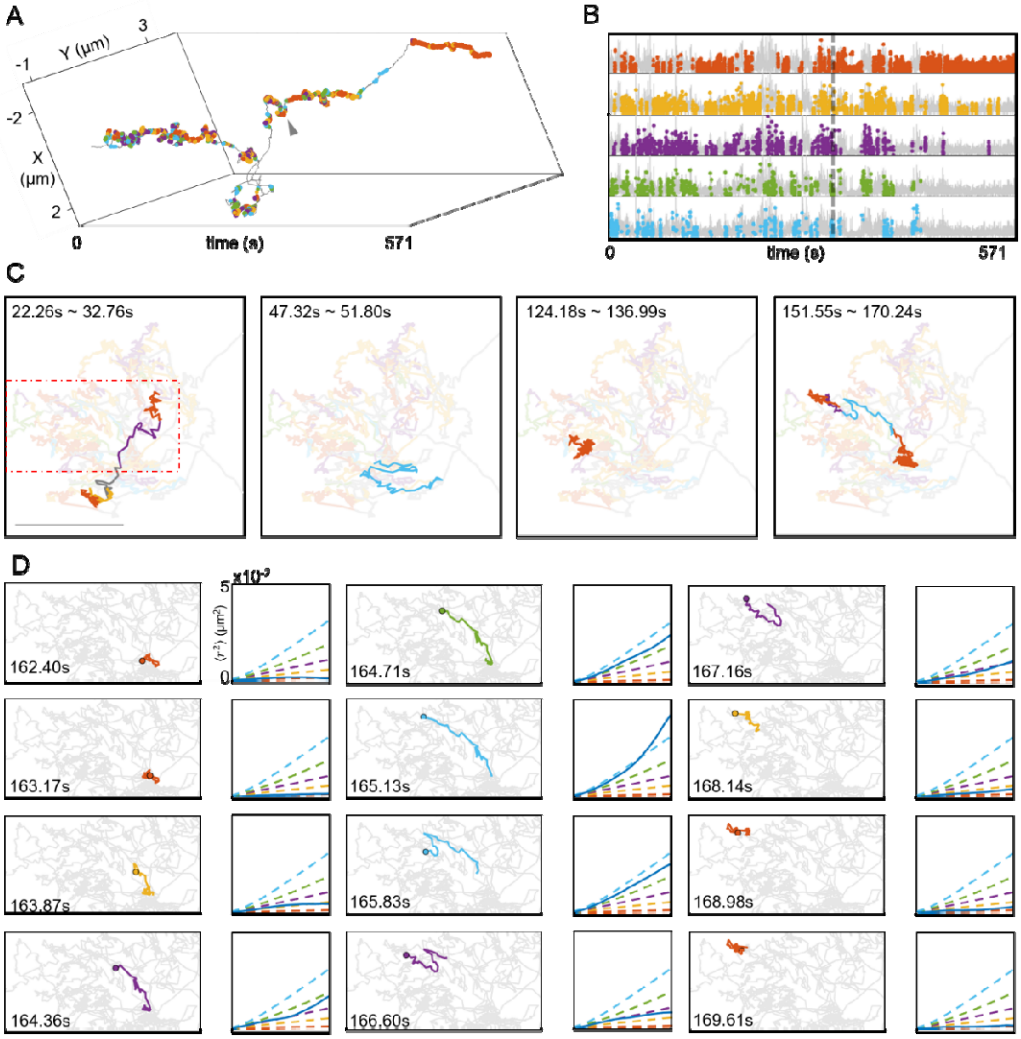

Fig10. Single AuNR diffusional states and transitions revealed by SEES operator. (A) The colored 3D spatiotemporal trajectory of the RGD-modified AuNR in Fig. 3 after SEES/MSD-ED operation on its velocity time series. (B) Temporal distribution of differently colored segments before and after the transmembrane site (dash line). The degree of confinement decreases from orange to blue. (C) Randomly selected 4 sets of segments show the hop-and-linger behavior of the AuNR as it searches for the cell-entry site in the first diffusive region (marked as blue in Fig. 3A and 3C insert). (D) Sequential evolution of some of the experience vectors in the red dash box in C. For each pair of the graphs, the left one is the spatiotemporal trajectory of the experience vector carried by the time point; the right one is the MSD curve (blue solid line) as compared to the 5 cluster centers (dashed lines).

Besides analyzing one trajectory from different perspectives, the SEES operator could process multiple trajectories of different characteristics simultaneously. As an example, we compared the cellular uptake of single AuNRs coated with RGD and cationic peptide, respectively. The later takes an electrostatic adsorption mediated internalization mechanism that is different from the receptor-mediated endocytosis pathway. For 2 set of trajectories of each case, we used SEES/MSD-ED, SEES/U-ED and SEES/AC-ED operator to analyze the local spatial confinement, motion speed and rotation rate of the 4 particles, respectively. By counting the number of different color points on each colored trajectory (Fig11.A), we obtained 12 state frequency histograms

representing the unique dynamic profiles of the single AuNR interacting with HeLa cell membrane (Fig11.B). While the cationic peptide-coated AuNRs covered a smaller membrane area, they have less lateral confinement, higher translation speed and faster rotation rate than the RGD-coated AuNRs, implying a smaller DLC dominated by weaker interaction between the cationic peptide and the cell membrane. RGD-coated AuNRs stayed longer durations at high DLC state and took more time to enter the cell. In contrast, cationic peptide-coated AuNRs displayed frequent transitions between high and low DLC states and spent less time on penetrating the cell membrane. These observations could be attributed to that the RGD-coated AuNRs suffer from gradually increased confinement due to multiple receptor-ligand binding before endocytosis, while the interaction between the cationic peptide-coated AuNRs and the negatively charged plasma membrane is governed by electrostatic interaction. The abundant information extracted from the multivariate trajectories could be beneficial to in-depth study of the diffusion dynamics of various nano-cargoes at the single particle level.

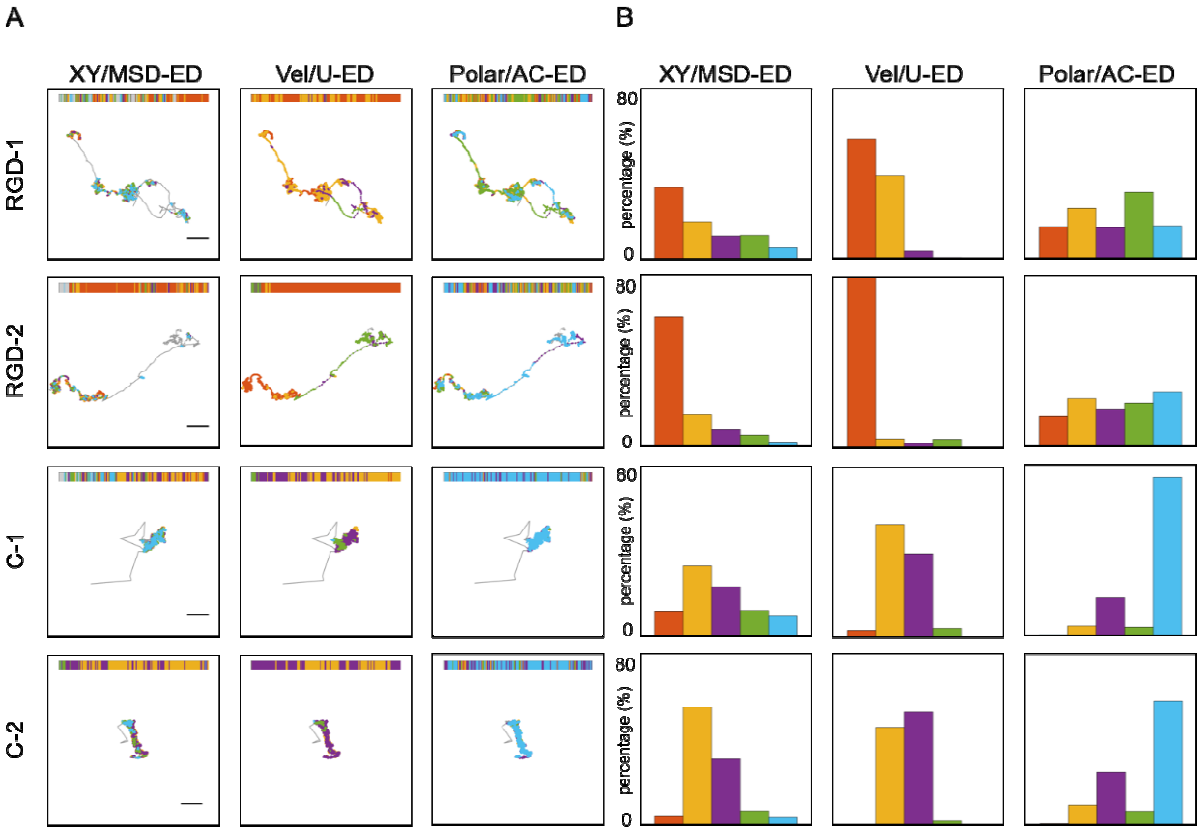

Fig11. Differential dynamics of RGD and cationic peptide modified NRs. SEES/MSD-ED, SEES/U-ED, SEES/AC-ED operators were applied to analyze the spatial positioning, velocity and polar angle of 2 RGD-modified AuNR (RGD-1 and RGD-2) and 2 cationic-peptide-modified AuNR (C-1 and C-2) transmembrane dynamics, respectively. (A) Each box shows the colored segmentation of the corresponding time series (color bar code insert) and its mapping onto the spatiotemporal trajectory. The scale bar is 1 μm. The length of all trajectories used here was 8000 frame (560s). (B) The group percentage profiles revealed by the corresponding operator.

5. Discussion

We have demonstrated through both simulation and experimental data analysis that the SEES operator is able to uncover the hidden motion mechanism or the inner differences embedded within the observed dynamics. Adopting the AuNR-cell membrane interaction for a case-study, we show that a combination of particle velocity, rotation angle and spatial position data can be readily analyzed using the same format without predefining a set of models and parameters for each differently recorded time series. This multivariate SPT analysis provides a comprehensive visual interpretation of the particle dynamics, and the resulting color labeling and segmentation of the trajectories make it convenient to identify the boundaries, transitions and critical points of the motion states of various functionalized NPs.

More generally, the trajectory of an individual particle can be considered as a time-course evolution in state space and thus comprise not only widely studied spatial coordinates but also other variates that describe the dynamics of the particle such as scatter light intensity and color under the microscope. As the imaging equipment and tracking algorithm developed rapidly, more dimensions of the variates as well as larger data set are obtained from a single experiment. Although the pre-defined physical model is essential to interpret data with limited size, this strategy may face its difficulty of “model explosion” in dealing with multivariate trajectory in state space, that is, the number of models and parameters needed to fully describe a certain particle dynamic increase extraordinarily versus the number of observed physical parameter. The SEES operation could be a complementary option to simply let the inner structure of the time series emerge by themselves without prior assumptions of the system, and therefore provide with both an intuitive picture and quantitative characterization of the multivariate trajectory by the same algorithm. The abundant information obtained from this presuppositionless method without averaging, fitting or oversimplification could be further used to inspire new knowledge finding, modeling or downstream biological/physical experimental evaluation. Therefore, this method could potentially help studies on heterogeneous individual dynamics, especially those lacking prior knowledge or multiple variates being observed.

The uniqueness of the SEES operation lies in the “negation” of the mechanical viewpoint on the acquired spatiotemporal data. Rather than viewing the data as mere assembly of isolated points, frame them with external a priori models, and try to establish an “objective description” of the complex system, we assign a short history to every data point, differ them based on the variation of their history, and tag them according to their classified history. Just like labeling protein or DNA biopolymers with fluorophores, coloring single particle trajectory with its own history exhibits a comprehensible representation of the original spatial or spatiotemporal structure. On the other hand, unlike static fluorescent labeling, dynamic historical labeling of a single particle trajectory is not exclusive. How to construct the history of the data point and how to compare the history determines how to color the trajectory. Nevertheless, as long as the SEES operation is reproducible, the resulting coloring profile is the truth of the spatiotemporal difference of the particle behavior, and the diversity of color labeling profiles reflects the complexity of particle dynamics and its surrounding environment. After all, no data would be meaningful if not being interpreted appropriately. Wherever relying on external models or internal historical comparison, some sort of subjective-objective unification is necessary during any data processing.

Besides analyzing the single particle trajectories, this data-phenomenology strategy provides a

general framework for spatiotemporal series analysis of complex systems aiming to reveal their interconnectivity and dynamic evolution. For decades, mechanical-model-based data-analysis and computer-simulation have played significant roles in advancing our understandings on the fundamentals and the prediction capability of system behavior in numerous research fields. On the other hand, the arbitrary division between the essential laws and the changing phenomena often restricts researchers from going deep into the water of complexity. Our approach, with no predefined external models and laws, provides a novel rationale that allows the underline mechanisms of complex systems to emerge on their own out of the otherwise huge amount of clueless data. The SEES operation meets the recent trend "to let data speak for themselves" in data science and could potentially inspire the finding of new knowledge of many systems. We expect that the unification of the phenomenology approach and data science will fundamentally promote the studies of the complexity issues.

Reference

1. S. T. Kim, K. Saha, C. Kim, V. M. Rotello, The Role of Surface Functionality in Determining Nanoparticle Cytotoxicity. Acc. Chem. Res. **46**, 681-691 (2013).
2. J. R. Baylis et al., Self-propelled particles that transport cargo through flowing blood and halt hemorrhage. Science Adv. **1**, e1500379 (2015).
3. Z. Cheng, A. Al Zaki, J. Z. Hui, V. R. Muzykantov, A. Tsourkas, Multifunctional Nanoparticles: Cost Versus Benefit of Adding Targeting and Imaging Capabilities. Science **338**, 903-910 (2012).
4. N. L. Rosi et al., Oligonucleotide-Modified Gold Nanoparticles for Intracellular Gene Regulation. Science **312**, 1027-1030 (2006).
5. T. T. Smith et al., In situ programming of leukaemia-specific T cells using synthetic DNA nanocarriers. Nat. Nanotechnol. **12**, 813-820 (2017).
6. S. Ohta, D. Glancy, W. C. W. Chan, DNA-controlled dynamic colloidal nanoparticle systems for mediating cellular interaction. Science **351**, 841-845 (2016).
7. A. von Diezmann, Y. Shechtman, W. E. Moerner, Three-Dimensional Localization of Single Molecules for Super-Resolution Imaging and Single-Particle Tracking. Chem. Rev. **117**, 7244–7275 (2017).
8. P. Liu et al., Rapid, directed transport of DC-SIGN clusters in the plasma membrane. Science Adv. **3**, eaao1616 (2017).
9. D. Xu, Y. He, E. S. Yeung, Direct imaging of transmembrane dynamics of single nanoparticles with darkfield microscopy: improved orientation tracking at cell sidewall. Anal. Chem. **86**, 3397-3404 (2014).
10. K. J. Lee, P. D. Nallathamby, L. M. Browning, C. J. Osgood, X.-H. N. Xu, In vivo imaging of transport and biocompatibility of single silver nanoparticles in early development of zebrafish embryos. ACS Nano **1**, 133-143 (2007).
11. Y. Gu, W. Sun, G. Wang, N. Fang, Single particle orientation and rotation tracking discloses distinctive rotational dynamics of drug delivery vectors on live cell membranes. J. Am. Chem. Soc. **133**, 5720-5723 (2011).
12. K. Chen et al., Characteristic rotational behaviors of rod-shaped cargo revealed by automated five-dimensional single particle tracking. Nat. Commun. **8**, 887 (2017).

13. H. M. Ding, Y. Q. Ma, Theoretical and computational investigations of nanoparticle-biomembrane interactions in cellular delivery. Small **11**, 1055-1071 (2015).

14. M. J. Saxton, Anomalous diffusion due to binding: a Monte Carlo study. Biophys. J. **70**, 1250-1262 (1996).

15. C. Metzner et al., Superstatistical analysis and modelling of heterogeneous random walks. Nat. Commun. **6**, 7516 (2015).

16. S. Huet et al., Analysis of Transient Behavior in Complex Trajectories: Application to Secretory Vesicle Dynamics. Biophys. J. **91**, 3542 (2006).

17. F. Persson, M. Linden, C. Unoson, J. Elf, Extracting intracellular diffusive states and transition rates from single-molecule tracking data. Nat. Methods **10**, 265-269 (2013).

18. S. T. Lownam et al., ErbB1 dimerization is promoted by domain co-confinement and stabilized by ligand-binding. Nat. Struct. Mol. Biol. **18**, 1244-1249 (2011).

19. J. A. Helmuth, C. J. Burckhardt, P. Koumoutsakos, U. F. Greber, I. F. Sbalzarini, A novel supervised trajectory segmentation algorithm identifies distinct types of human adenovirus motion in host cells. J. Struct. Biol. **159**, 347-358 (2007).

20. T. Wagner, A. Kroll, C. R. Haramagatti, H. G. Lipinski, M. Wiemann, Classification and Segmentation of Nanoparticle Diffusion Trajectories in Cellular Micro Environments. PLoS One **12**, e0170165 (2017).

21. N. Monnier et al., Bayesian approach to MSD-based analysis of particle motion in live cells. Biophys. J. **103**, 616-626 (2012).

22. M. R. Kelly, Phenomenology and Time-Consciousness, https://www.iep.utm.edu/phe-time/.

23. R. García-Gavilanes, A. Mollgaard, M. Tsvetkova, T. Yasseri, The memory remains: Understanding collective memory in the digital age. Science Adv. **3**, e1602368 (2017).

24. N. Pržulj, N. Malod-Dognin, Network analytics in the age of big data. Science **353**, 123-124 (2016).

25. N. B. Turk-Browne, Functional Interactions as Big Data in the Human Brain. Science **342**, 580-584 (2013).

26. L. Einav, J. Levin, Economics in the age of big data. Science **346**, 715-715 (2014).

27. B. Shneiderman, The Big Picture for Big Data: Visualization. Science **343**, 730-730 (2014).

28. L. Cao, Practical method for determining the minimum embedding dimension of a scalar time series. Physica D **110**, 43-50 (1997).

29. A. M. Fraser, H. L. Swinney, Independent coordinates for strange attractors from mutual information. Phys. Rev. A **33**, 1134-1140 (1986).

30. A. Rodriguez, A. Laio, Clustering by fast search and find of density peaks. Science **344**, 1492-1496 (2014).

31. E. Keogh, J. Lin, Clustering of time-series subsequences is meaningless: implications for previous and future research. Knowl. Inf. Syst. **8**, 154-177 (2005).

32. K. Yang, Y. Q. Ma, Computer simulation of the translocation of nanoparticles with different shapes across a lipid bilayer. Nat. Nanotechnol. **5**, 579-583 (2010).

33. K. Suzuki, K. Ritchie, E. Kajikawa, T. Fujiwara, A. Kusumi, Rapid hop diffusion of a G-protein-coupled receptor in the plasma membrane as revealed by single-molecule techniques. Biophys. J. **88**, 3659-3680 (2005).

Supporting Information

Note S1. The Description of the SEES operator

The algorithm of the SEES operator implemented by MATLAB script mainly consists of three parts, the construction of the historical experience vector, the unsupervised clustering and results viewer based on the color code mapping corresponding to the three steps described in the manuscript. For time series observations of a particle dynamics:

$$\boldsymbol{M_i} = \{m_1, m_2, \dots, m_N\}$$

$$\boldsymbol{R_i} = \{\vec{r}_1, \vec{r}_2, \dots, \vec{r}_N\} = \{(x_1, y_1), (x_2, y_2), \dots, (x_N, y_N)\}$$

The $\boldsymbol{M_i}$ is the time series observation such as velocity or rotation angle while the $\boldsymbol{R_i}$ represents the time series of the particle locations. Time intervals between consecutive observations is Δt. The historical experience-vector can be constructed by 3 means provided by the algorithm:

1. Univariate method

$$\boldsymbol{V}_i^{\tau,d} = \left(m_{i-(d-1)\tau}, m_{i-(d-2)\tau}, \dots, m_i\right)$$

2. MSD method

$$\boldsymbol{V}_i^{\tau,d} = (\langle {r_i}^2\rangle_{\Delta t}, \langle {r_i}^2\rangle_{2\Delta t}, \dots, \langle {r_i}^2\rangle_{\mathrm{d}\Delta t})$$

$$\langle {r_i}^2\rangle_{\mathrm{n}\Delta t} = \frac{1}{2d-n}\sum_{j=0}^{2d-n-1}\left|\vec{r}_{i-j} - \vec{r}_{i-j-n}\right|^2$$

3. Autocorrelation method (AC)

$$\boldsymbol{V}_i^{\tau,d} = \left(c_i^0, c_i^1, \dots, c_i^\tau\right)$$

$$c_i^j = \frac{(d-j)\sum_{k=0}^{d-j-1}(m_{i-k}m_{i-j-k}) - \sum_{k=0}^{d-j-1} m_{i-k}\sum_{k=0}^{d-j-1} m_{i-j-k}}{(d-j)\sqrt{\sum_{k=0}^{d-j-1}(m_{i-k})^2 - (\sum_{k=0}^{d-j-1} m_{i-k})^2}\sqrt{\sum_{k=0}^{d-j-1}(m_{i-j-k})^2 - \left(\sum_{k=0}^{d-j-1} m_{i-j-k}\right)^2}}$$

Here, $\boldsymbol{V}_i^{\tau,d}$ represents a historical experience-vector constructed in the first step and anchored at a specific time point *i*. For each construction method, an initial offset is required as the beginning of the series, where the historical experience detected is shorter than the length of the vector and hence invalid. The offset for the univariate, MSD and AC methods are $1 + (\mathrm{d} - 1)\tau$, 2d and d respectively. The entire sequence of the constructed experience-vectors can be represented as a matrix $\boldsymbol{W}$ and is ready for the following unsupervised clustering.

The univariate and AC method are suitable to deal with single time series variable $\boldsymbol{M}$ while MSD method is meant to handle spatial movement series which has the two $\boldsymbol{X}$ and $\boldsymbol{Y}$ coordinates. Univariate method is helpful to extract historical experience variation values in the time series, while the AC method mainly focuses on the fluctuation properties of the series. The MSD method is suitable to investigate the historical confinement experience as its physical definition indicates.

In the next step, the experience-vectors are compared globally to let the internal differences emerge. Here, to prove the concept, we adopted the k-means clustering, which is one of the most widely used unsupervised clustering algorithms, as our classifier. Similarity measurement can be performed with various metrics to focus on different features of the vector. The metrics we adopted here include Euclidean (ED), Cross-Correlation (CC), and Minkowski Distance (p=5, MD).

$$S_{(i,j)}^{ED} = \sqrt{(\boldsymbol{V}_i - \boldsymbol{V}_j)(\boldsymbol{V}_i - \boldsymbol{V}_j)'}$$

$$S_{(i,j)}^{CC} = 1 - \frac{(\boldsymbol{V}_i - \langle \boldsymbol{V}_i \rangle)(\boldsymbol{V}_j - \langle \boldsymbol{V}_j \rangle)'}{\sqrt{(\boldsymbol{V}_i - \langle \boldsymbol{V}_i \rangle)(\boldsymbol{V}_i - \langle \boldsymbol{V}_i \rangle)'}\sqrt{(\boldsymbol{V}_j - \langle \boldsymbol{V}_j \rangle)(\boldsymbol{V}_j - \langle \boldsymbol{V}_j \rangle)'}}$$

$$S_{(i,j)}^{MD} = \sqrt[p]{\sum_{k}^{n} \left| V_{ik} - V_{jk} \right|^p}$$

The metric selection helps us to focus on different aspects of the experience vector. CC metric is sensitive to the variation trend of the sequence of elements in the vector, while the ED and MD metrics mainly focus on the magnitude of the vector elements. As the MD is a generalized form of the ED, their clustering results are often comparable to each other. In MD metric we set p=5 as an odd number to make this metric more robust to fluctuations. To meet more specific needs, more advanced metric such as DTW[1,2] can also be adopted in the clustering step. Considering both the experience vector construction and the metric selection, theoretically we can provide 9 different combinations in the algorithm. With the univariate method (U), the U-ED/U-MD combination is capable of differentiating the magnitude of experience vector of a specific measurement, such as the velocity or angle variation of the AuNRs. Meanwhile the U-CC combination is suitable to differentiate the historical tendency like what we did in the double-sinusoidal model in Figure 2a. AC curve usually works with ED metric to differentiate the historical fluctuation behavior such as the rotation dynamics of the AuNRs as it always exhibits similar decade tendency. MSD-ED/MSD-MD consider the magnitude of historical mean displacement versus the increasing time interval while MSD-CC only consider the tendency of the curve growing.

In this work, we use the basic and well-studied k-means method to perform the clustering. Again, more advanced clustering methods or cluster number estimation method can be applied in this step. Here, we optimize the performance of the classical k-means by two ways. First, multiple runs were used to reduce the interference due to the random initiation, optimized result was selected by the minimal sum of sample-cluster-center distance. Meanwhile, rare cluster whose population is lower than a threshold (usually 10%~20%) was marked as undefined group to ignore the effect of outliers.

After classification of the historical experience-vectors, the original spatiotemporal trajectory or the time-series of the AuNR velocity or angle were colored according to the clustering results. Besides providing an overall color segmentation pattern, an algorithm is designed to identify the exact frame-wise positions of each same color segment. To eliminate too short noise segments, we set up a 20-frame-length (1.4 s) threshold. A segment shorter than 20 frames would be combined into the following one until its length reaches 20-frames. Several visualization methods were implemented in MATLAB as well to enable the researchers to navigate the spatiotemporal series step by step and get an intuitive picture of the collective dynamics.

The main function of the MATLAB codes is pNPa which returns a NPMotionTest instance containing all the data-processing results. The visualization was performed by PNPGUI class which accepts a NPMotionTest instance and then generate a user-friendly GUI interface. The user can easily navigate around along the whole trajectories to

catch the dynamic details as well as the spatiotemporal patterns as a whole. The calling formats of these functions are:

$$\mathrm{NPMotionTest} = \mathrm{pNPa}(xy, rawData, method, param, comd, optTime, isSpeak, minGroupSize)$$

$$\mathrm{PNPGUI\ instance} = \mathrm{PNPGUI}(NPMotionTest\ instance)$$

More description of the function options can be found in the table below.

Parameter descriptions of the functions.

Input parameter	Explanations
xy	particle trajectory formatted as **N×2 matrix**, each row is a XY coordinate observed at specific time
$rawData$	processing raw data, the valid format depends on the $method$ (Table 2)
$method$	the method for historical vector extraction, a **String** variable
$param$	a 1×4 vector parameter for historical vector extraction, see Table 3.
$comd$	cluster metric, a **char** variable. **E** for Euclidean Distance, **C** for Corss-Correlation and M for Minkowski Distance.
$optTime$	cluster repeating time. Each time the algorithm converges in a local optimization. Repeat with randomly initial state helps to obtain global optimization, a **scalar number**.
$isSpeak$	is plot the result at the end of processing, a **logical** variable
$minGroupSize$	constrain the minimum number of group members in cluster to avoid the outliers effect. a **fraction** number.

Supplementary Note S2. Model simulation.

1. The rotation/revolution model. The rotation/revolution model was simulated by combining two sinusoidal functions with different frequencies.

$$\mathrm{y(t)} = \sin\left(\frac{t}{10}\right) + \sin(t) + N$$

Here, the ***N*** represents a standard normal distributed random noise.

2. Random walk on heterogeneous 1D cell membrane. A virtual 1D cell membrane was set ranging from -∞ to +∞ and served as the default region. Then, several specific local regions were added with heterogeneous properties. The local properties of a specific region of the simulated cell membrane consist of the local diffusion coefficient $\boldsymbol{d_t}$ and direction preference ***p***. The direction preference provides a bias of the direction selection in random walk. $\boldsymbol{p} \in [-1,1]$ where -1 means absolute negative movement and +1 means absolute positive movement. The step length was generated as following:

$$l \sim N(0, 2d_t\Delta\mathrm{t})$$

where $\Delta\mathrm{t}$ is the time interval of the simulation. The particle was placed at a specific coordinate and then allowed to diffuse based on its local regional properties. The expectation of the particle velocity is given by:

$$\mathrm{E}(|v|) = \sqrt{\frac{4d_t}{\pi\Delta t}}$$

3. State switching on 2D cell membrane. The 2D cell membrane was generated with an enclosed boundary and a specific diffusion coefficient $d_{t,0}$. Then, a number of non-overlapped binding sites were placed randomly on the cell membrane. For each binding site i, four parameters were used to specify its binding behaviors: confined radius r_i, local diffusion coefficient $d_{t,i}$, affinity coefficient a_i and escape probability p_i. The particle initiated on the membrane with Brownian motion. After entering a certain binding site, the particle can alter its state to the binding state according to the affinity coefficient of the site. In binding state, the particle movement in each step was divided into 100 sub-steps and make sure that the particle is confined inside the binding radius. After each confined step, the particle can take a chance to release itself and transform to directed motion according to the escape probability. The motion step length was generated according to the density function[3] F_l:

$$F_l(l) = \frac{2l}{4d_t\Delta t} e^{\frac{-l^2}{4d_t\Delta t}}$$

The directed motion was simulated by direction restriction:

$$\frac{v_{i+1} \cdot v_i}{|v_{i+1}||v_i|} < \theta$$

Supplementary Note S3. Estimate out-of-plane angle of AuNR

After adding the functionalized AuNRs into the cell culture medium, we examined the dynamic interactions between single AuNRs and the cell under darkfield microscope equipped with a color CCD camera. Thanks to the anisotropic plasmonic properties, the scattering color for one AuNR is dependent on its spatial orientation, allowing us to achieve single particle translational and rotational tracking. With this technique, we studied the dynamic interaction between single AuNRs and the cell in real time and obtained the consequent behavior pattern changes from the long-term rotational and translational trajectories. Under darkfield microscope, the color of single AuNRs detected by the DP72 color CCD camera can be described as

$$[R, G, B] = \int_{400}^{700} I(\lambda) \cdot P_a \cdot P_s \cdot [R(\lambda), G(\lambda), B(\lambda) \cdot d\lambda$$

where I(λ) is the spectrum of the light source, R(λ), G(λ) and B(λ) represent the response curves of the color detectors, Pa and Ps are the efficiency of absorption and scattering of AuNRs respectively.

For the AuNRs illuminated under darkfield microscopy using a darkfield condenser (with NA = 1.2~1.4), the angle (ξ) between the incident light with XY plane where the AuNR located ranges from 64.5° to 90°. Then the efficiency of absorption of AuNR can be given by[4]

$$P_a = \frac{\int_{1.1257}^{1.5707} \sin\xi \cdot d\xi}{\int_{1.1257}^{1.5707} d\xi} = 0.9673$$

For the red channel, the efficiency of scattering can be obtained from the projection of scattering cross sections of the dipoles of the AuNR in XY plane,

$$P_{s,1} = C_{S1} \cdot \sin^2\theta + C_{S2} \cdot \sin^2\left(\frac{\pi}{2} - \theta\right) + C_{S3}$$

where the C_{S1}, C_{S2} and C_{S3} are the scattering cross section of the three dipoles of the AuNR (1 indicates the longitudinal plasmonic dipole, 2 and 3 are the two transversal plasmonic dipoles of the AuNR, with $C_{S1} > C_{S2} = C_{S3}$), θ is the polar angle of the AuNR.

For the green channel, the direction of X axis was appointed as the direction of the polarizer and then the efficiency of scattering of AuNR can be obtained from the following expression,

$$P_{s,2} = C_{S1} \cdot \sin^2\theta \cdot \cos^2\phi + C_{S2} \cdot \sin^2\left(\frac{\pi}{2} - \theta\right) \cdot \cos^2\phi + C_{S3}$$

According to the above equations, the RGB values of each AuNR in the two channels detected by the color camera in our imaging system are dependent on the polar angle θ and azimuth angle □ (Figure S5 simulated results). With the aid of boundary conditions at θ = 0° and θ = 90°, the polar angle can be obtained from the intensity in the red and green channels,

$$\sin^2\theta = f(R, G) = \frac{(R - G) - (R - G)_{min}}{(R - G)_{max} - (R - G)_{min}}$$

The R and G are the color of the scattering spots. By integrating the single-particle tracking technique, both the rotational and translational motions of single AuNRs that interacting with live cells can be readily resolved with the darkfield microscopy.

Reference

1 Chen, Y., Hu, B., Keogh, E. & Batista, G. E. A. P. A. in *ACM SIGKDD International Conference on Knowledge Discovery and Data Mining*. 383-391.

2 Deng, H., Runger, G., Tuv, E. & Vladimir, M. A time series forest for classification and feature extraction. *Information Sciences* **239**, 142-153, doi:10.1016/j.ins.2013.02.030 (2013).

3 Wagner, T., Kroll, A., Haramagatti, C. R., Lipinski, H. G. & Wiemann, M. Classification and Segmentation of Nanoparticle Diffusion Trajectories in Cellular Micro Environments. *PLoS One* **12**, e0170165, doi:10.1371/journal.pone.0170165 (2017).

4 Xu, D., He, Y. & Yeung Edward, S. Direct Observation of the Orientation Dynamics of Single Protein□Coated Nanoparticles at Liquid/Solid Interfaces. *Angewandte Chemie* **126**, 7071-7075, doi:10.1002/ange.201400025 (2014).

5 Matthews, B. W. Comparison of the predicted and observed secondary structure of T4 phage lysozyme. *Biochimica et Biophysica Acta (BBA) - Protein Structure* **405**, 442-451, doi:https://doi.org/10.1016/0005-2795(75)90109-9 (1975).

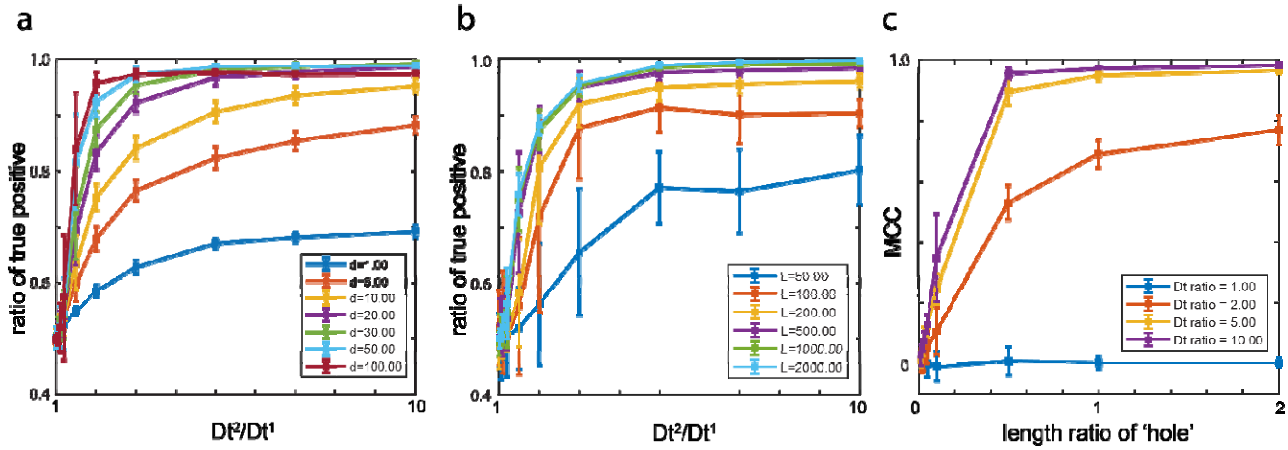

Figure S1 | Performance validation of the SEES operator. Brownian random walk segments with different diffusion coefficient (D_t) were merged together to evaluate the accuracy of SEES operator. All measurements were repeated 30 times, the error bar shows standard deviation of the results. (a) Two equal length of the segments with different ratio of Dt were tested under different historical experience vector length d. The differentiation accuracy was measured by the ratio of true position. Low experience vector length (d=1, blue) shows relative low accuracy even in high Dt ratio, while d=30~50 show the best performance. Long experience vector length (d=100, dark red) shows slightly lower accuracy. (b) The same test as in a with fixed d=30 and different segment length. Short segment length (L=50, blue) shows unstable results and relative low accuracy. After the segment length reaches to 500 frames, the accuracy become satisfactory with $D_t^2/D_t^1 \geq 3$. (c) small segment with higher diffusion coefficient was inserted in a homogeneous random walk segments. The differentiation accuracy was measured by Matthews Correlation Coefficient (MCC) to address the unbalance binary classification issue, in which the fraction of correction measurement can be missleading[5]. Random results give approximately zero value of MCC as the performance in D_t ratio = 1 group (blue), which means the diffusion coefficient of the inserted segment is equal to that of the original segments. D_t ratio higher than 5 and length ratio higher than 0.5 gives satisfactory results (MCC ~ 1).

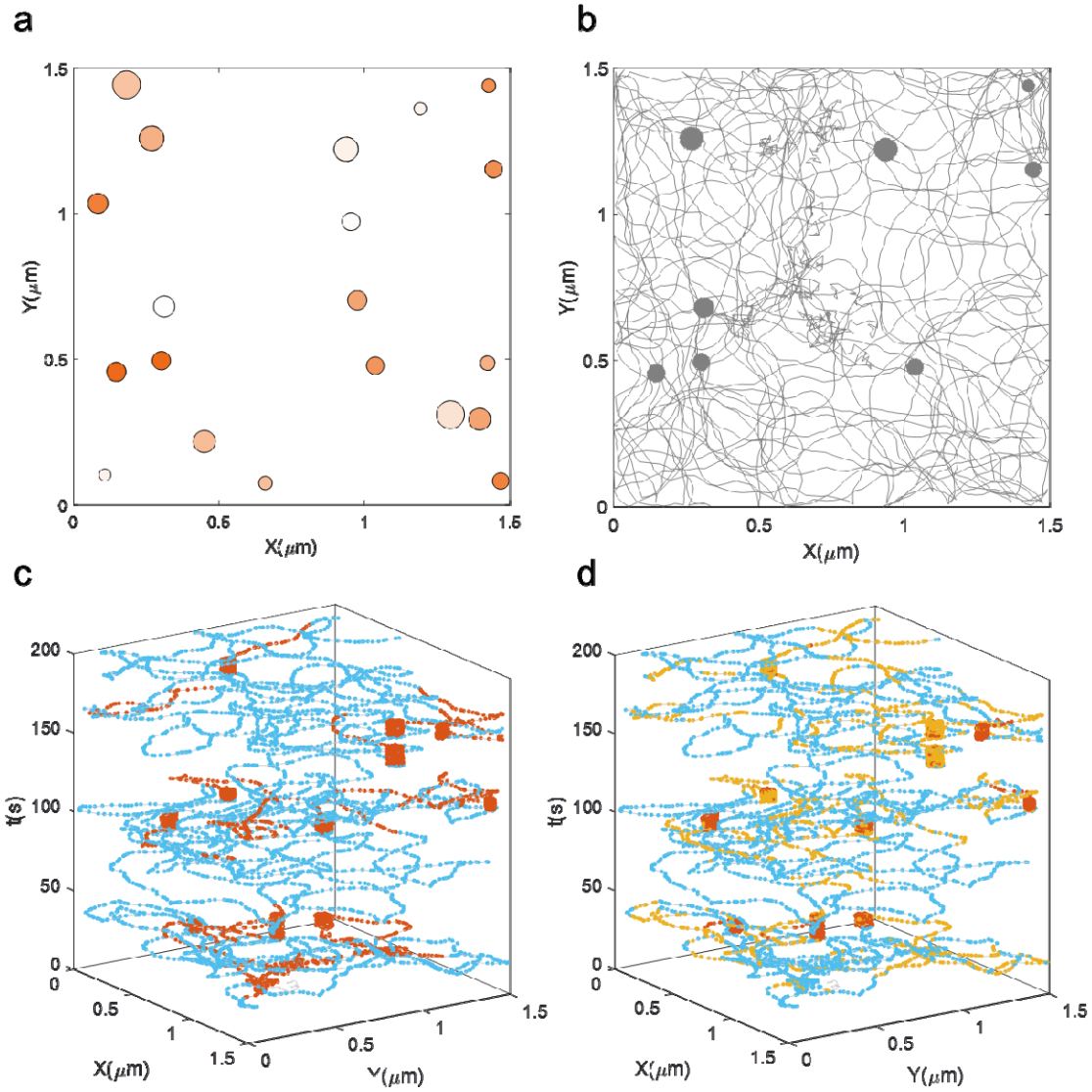

Figure S2 | Different SEES operators reveal various underlying mechanism. (a) The simulated ground truth of the 2D cell membrane in Figure 2E. The red circles represent the binding site on the membrane. Different color indicates the variations of the local diffusion coefficient of each binding site. The dark red stands for small diffusion coefficient while the light red represents large diffusion coefficient. (b) The simulated trajectory. (c) SEES/MSD-ED operation differentiates the binding state from the directed state. (d) SEES/U-ED operation reveals the local diffusion coefficient differences among binding sites (indicated by black arrow).

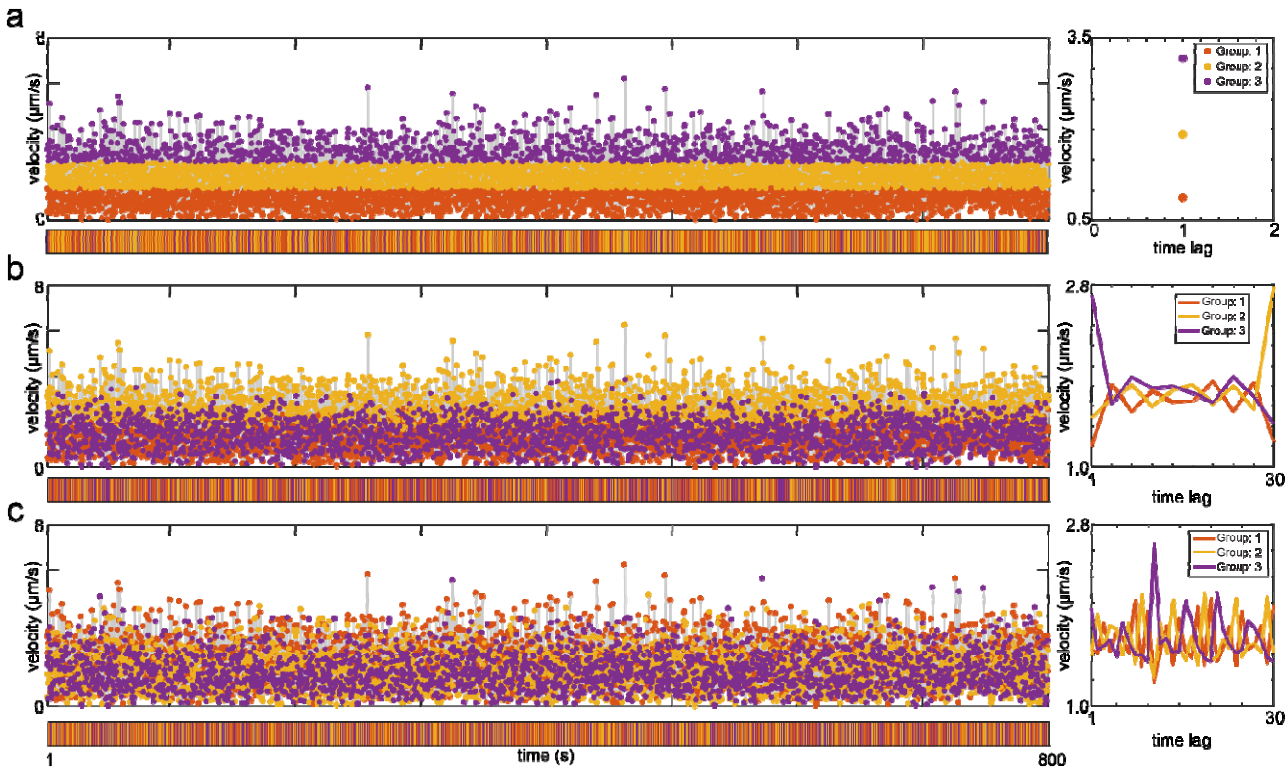

Figure S3 | SEES operation on pure homogeneous random-walk time-series. The same parameters were used as those applied in Figure 2D. Instead of assembling locally and forming colorful multiple segments as what happen in Figure 2D, the same color points randomly distributed along time, regardless of the length of the experience-vectors. Furthermore, the cluster centers shown on the right also imply that there is no certain patterns found. Therefore, the collective pattern emerge with SEES operation can only originate in the underlying mechanism of the time-series data themselves but not from the clustering algorithm.

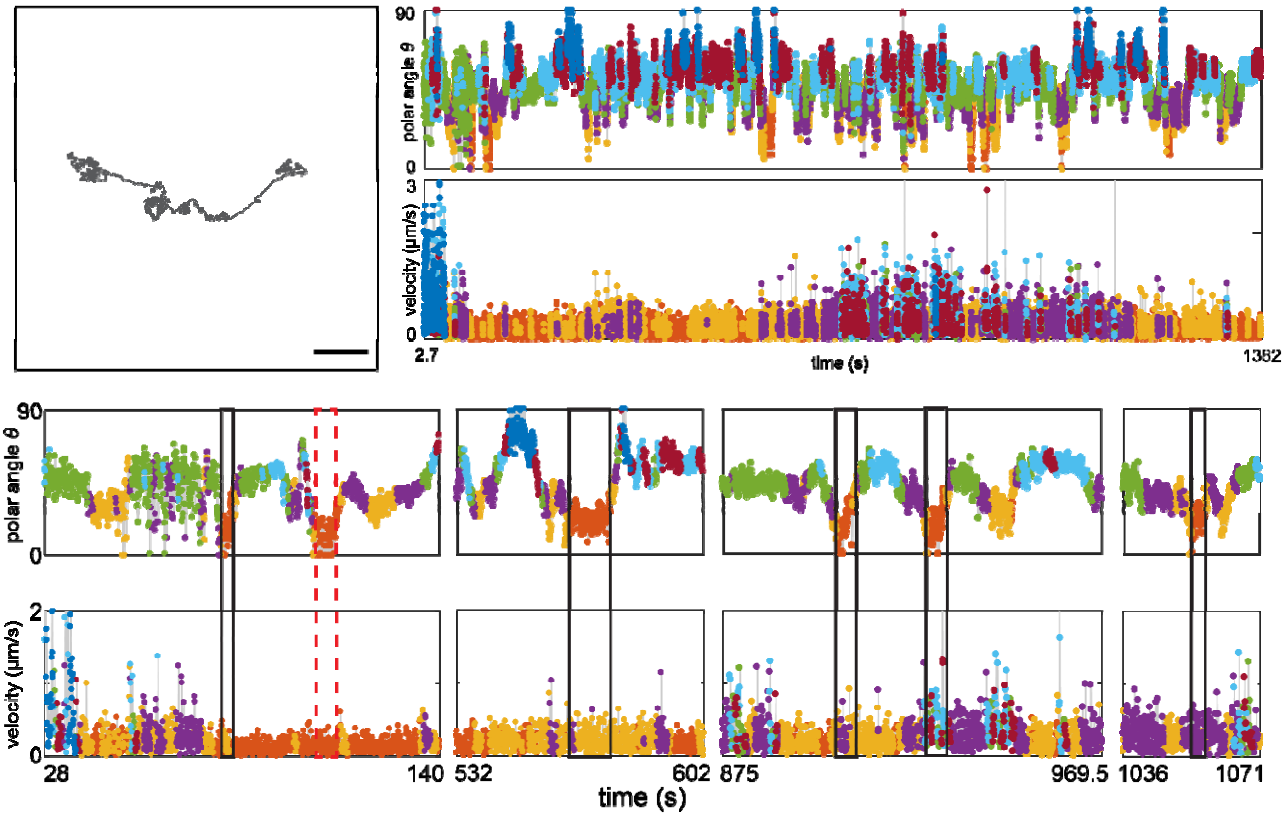

Figure S4 | SEES/U-ED operation for cell-entry point determination of the transmembrane process of another RGD-coated AuNR. (a) The untagged trajectory. The scale bar is 3 μm. (b) The color tagged time-series and collective pattern of polar-angle (top) and velocity (bottom) variation. (c) As described in the manuscript for Figure 3B, the cell-entry-point was identified by the overlapping of same orange color in the polar-angle series and velocity series, implying the co-localization of the highest confinement, vertical particle orientation and lowest motion speed. The one with the red-dash-box shows the only perfect occurrence of this synchronization. Others are similar but failed trial sites.

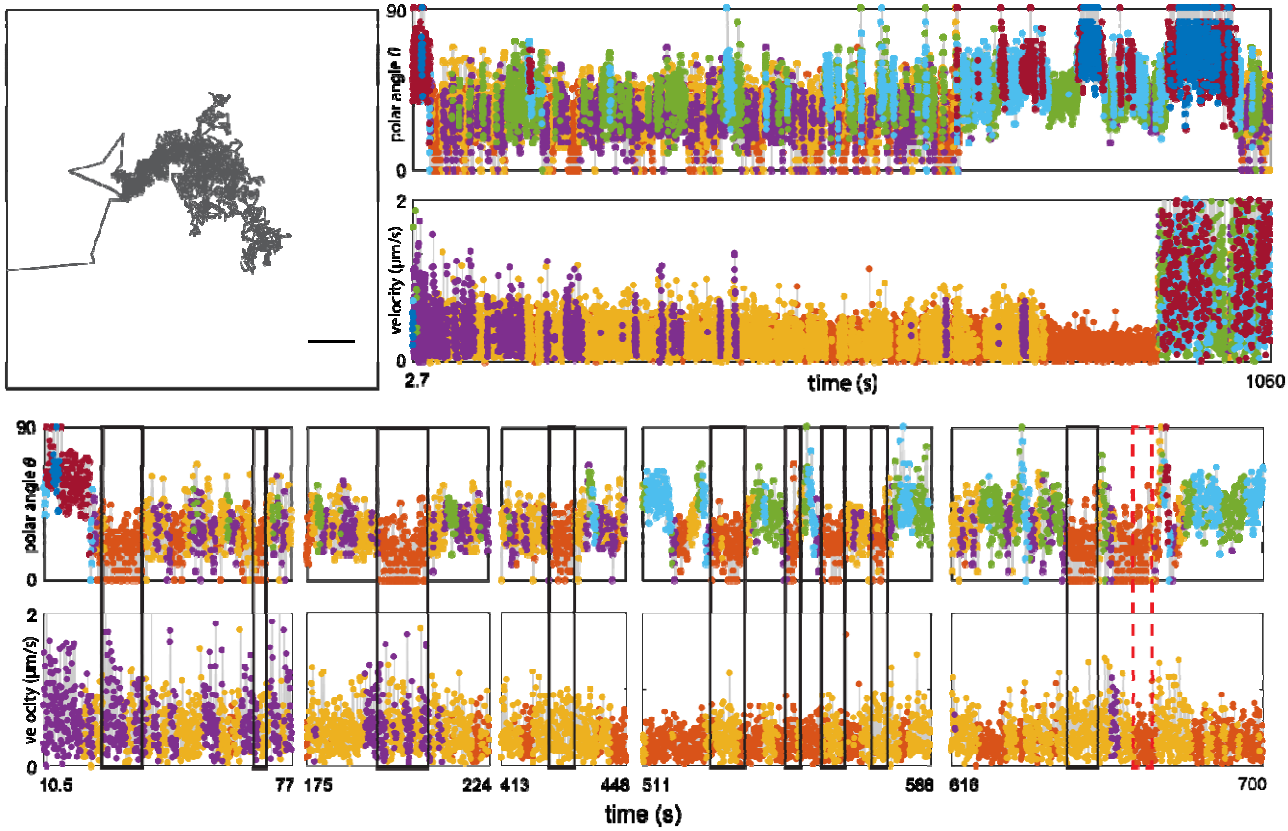

Figure S5 | SEES/U-ED operation for cell-entry point determination of the transmembrane process of a cationic peptide coated AuNR. The scale bar is 1 μm.

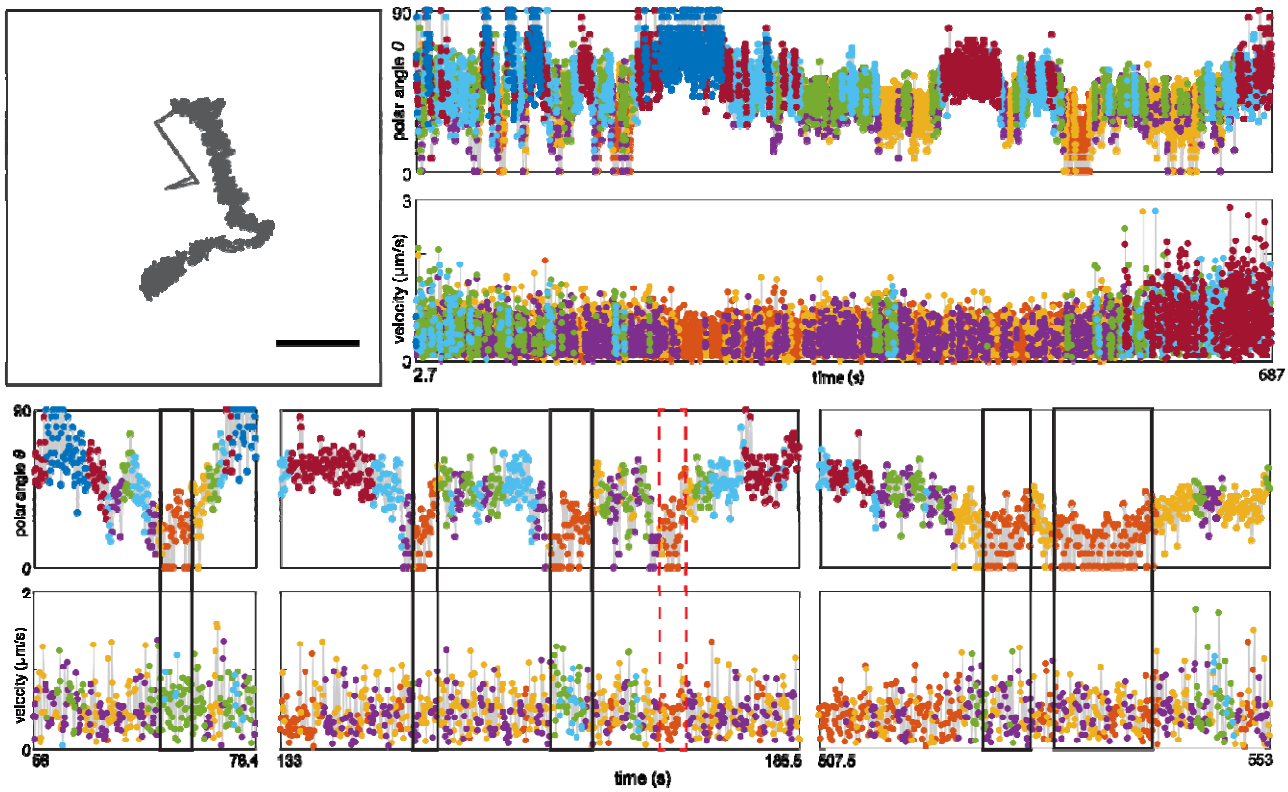

Figure S6 | SEES/U-ED operation for cell-entry point determination of the transmembrane process of another cationic peptide coated AuNR. The scale bar is 1 μm.